Finite Element Modeling of a Thawing Pavement Structure

Robert Haehnel, Sally Shoop, Rosa Affleck & Vincent Janoo
US Army Engineer Research and Development Center, Cold Regions Research and Development Laboratory (ERDC-CRREL), Hanover, NH, USA.

ABSTRACT: A material model for soft soil was developed to simulate the deformation behavior of a thawing soil under vehicle loading on paved and unpaved roads. Freeze–thaw action produces a loose, wet soil that deforms significantly under vehicle loads. The material model represents a frost–susceptible fine sand, which was used in full-scale tests of paved and unpaved road sections in CRREL's Frost Effects Research Facility (FERF). The material model was fine-tuned using triaxial test data and validated against direct shear test data. The material model was then used in a dynamic, three-dimensional finite element simulation of a paved road structure subjected to vehicle traffic by loading from a rolling wheel. This was used to understand the effects of thaw on the degradation of paved roads. These initial findings show that the pavement layer experiences maximum stress when the base layer is thawing. This supports observations that the majority of the rutting of a pavement system occurs during the thaw cycle.

KEYWORDS: Thawing, soil, pavement, roads, airfields.

1 INTRODUCTION

Spring thaw is a critical time for the deterioration of roads and airfields. Predicting how pavement structures will perform and deteriorate is important for scheduling maintenance and planning military deployments. In developing nations, the use of secondary roads and airfields for rapid deployment will be critical, and the performance of these structures must be understood and optimized.

A road surface (either paved or unpaved) will deform during spring thaw nearly always because the thawing layer, which has reduced density and is often very wet or saturated as a result of the freezing process, deforms. Large deformations can lead to failure (e.g., rutting and cracking) of the paved surfaced (Figure 1). This thaw weakening of pavement structures has been documented experimentally by Saarelainen et al (1999), Zhang and Macdonald (2002), Janoo and Berg (1990a, b), and Janoo and Shoop (2004); however, controlled, detailed study through finite element analysis is lacking. The weak, thawing layer deforms plasticly, consisting of both compaction and shear. Because the thickness of the thawing layer varies throughout the thawing season (during spring or intermittent thaws), a method to simulate both the plastic deformation and the various layering geometry was desired. Shoop et al. (2005) determined that the behavior of a thawing soil could be described using the well know Capped Drucker-Prager (CDP) constitutive law. Using triaxial test data, Shoop et al. derived the appropriate CDP material parameters and implemented this in a finite element

model. In this effort, we build on this previous work by validating the model on a more rigourous geometry: the direct shear test. Finally, we use the model to study distress of pavement systems during a thaw cycle.

Figure 1: Longitudinal rutting and cracking of a paved road due to thaw weakening of the supporting soil structure. Photo courtesy of Hannele Zubeck.

2 MODIFIED CAP DRUCKER-PRAGER MODEL

A thawing soil loses compaction through the freezing process, whereby excess water is drawn to the freezing front and expands, forming ice lenses. Also, the loose material is often wet or saturated during thaw, as water is trapped in the thawing layer by the impermeable frozen layer below. This material deforms plastically in both compaction and shear; this must be adequately represented by the material constitutive model.

Here we used the Modified Capped Drucker-Prager (CDP) constituative law, as implemented in the ABAQUS finite element code (HKS 1998), to model the behavior of thawing soil. The CDP model is thoroughly described in Shoop et al. (2005) and HKS (1998). To summarize, the CDP model has the features of a critical state model(i.e. regions of constant volume shear deformation, and compactive-dilatant flow). CDP uses non-associative flow on the shear surface (i.e. the flow potential is not associated with the yield surface) and associated flow on the cap surface.

The yield surface for the CDP material model is described in terms of stress invariants, p and t, of the stress tensor, where p is the equivalent pressure stress and t is the deviatoric stress. The yield surface is defined in the p-t plane (meridinal plane) and has two major segments: (1) the Drucker-Prager portion of the curve (analogous to the Mohr-Coulomb line) defines shear deformation, and (2) the cap portion of the surface defines the intersection with the pressure axis. The following equations define the yield criteria in each section of the yield surface. For Drucker-Prager shear or distortional failure

$$F_s = t - p\tan\beta - d = 0 \qquad (1)$$

where d is the Drucker-Prager material cohesion and β is the Drucker-Prager material angle of friction. These are analgous to Mohr-Coulomb cohesion, c, and the internal angle of friction, ϕ.

For the cap region of compactive-dilatant failure

$$F_c = \sqrt{(p - p_a)^2 + \left[\frac{Rt}{(1 + \alpha - \alpha / \cos\beta)}\right]^2} - R(d + p_a \tan\beta) = 0 \quad (2)$$

where α is a transition parameter, ranging typically from 0.0 to 0.05, that smooths the transition between the shear failure and the cap failure. In our thawing soil model, we use α = 0, i.e., there is no transition surface imposed. R, the cap eccentricity parameter, is a material parameter that controls the shape of the cap, and p_a is the intersection of the shear line and the cap (in absence of a transition surface) and relates to the cap hardening behavior according to

$$p_a = \frac{p_b - Rd}{(1 + R\tan\beta)} \quad (3)$$

where the mean hydrostatic pressure, p_b, is a function of the volumetric plastic strain, ε_{vol}^{pl}. This functional relationship, $p_b = f(\varepsilon_{vol}^{pl})$, is the hardening law that defines the pressure-volume relationship during compression of the material at the cap failure surface.

The pressure-volume relationship defines both hardening and softening through volume changes based on how the cap portion of the yield surfaces expands and contracts. The cap is generally spherical or ellipsoidal, and the material either hardens or softens by expanding or contracting the cap. This behavior is defined in a pressure-volume relationship called a hardening law. We represented the hardening law using a piecewise linear approach using the experimental data as a table of p_b and ε_{vol}^{pl} pairs.

The plastic flow is defined by an elliptical shaped, flow potential surface. Flow is associative (normal to the surface) in the cap region; therefore, the equation for the flow surface is identical to the equation for the cap yield surface. In the transition and shear region, the flow is non-associative (flow potential is independent of the failure surface), and the flow surface, G_s, is defined as (HKS 1998)

$$G_s = \sqrt{\left[(p_a - p)\tan\beta\right]^2 + \left[\frac{t}{1 + \alpha - \alpha / \cos\beta}\right]^2}. \quad (4)$$

3 SOIL MATERIAL

The soil material modeled in this study is Lebanon sand. Laboratory frost heave tests define this as a highly frost-susceptible material and according to the Unified Soil Classification System (USCS) it is a silty sand (SM). The soil was used in full-scale tests of paved and unpaved road test sections in the FERF. The material grain size distribution is given in Shoop et al. (2005). The soil is non-plastic (PI=0) and has a maximum density of 1856 kg/m^3 at an optimum moisture content of 12% (ASTM D 1557 Modified Proctor Test). This soil is well characterized for moisture migration during freeze–thaw (Shoop and Bigl 1997), for frost heave (Shoop and Henry 1991), in terms of *in-situ* shear strength (Shoop 1993) and triaxial testing on frozen cores (Shoop 1988). Additional data for this soil material are given in Shoop et al. (2005).

The CDP model parameters were determined from triaxial compression tests and hardening response of the soil was determined from hydrostatic consolidation tests (Shoop et al. 2005). These parameters and the hardening law for Lebanon sand are summarized in Table 1. The parameter, K, in Table 1 has not been previously defined and is the ratio of the tensile strength of the material to the compressive strength. In the absence of data to determine this parameter, it is recommended that a value of 1.0 be used (HKS 1998). We followed these recommendations.

Table 1: Material parameters and hardening table for the Modified Capped Drucker–Prager model of Lebanon Sand.

Material Parameter	
E, Young's modulus, kPa	8500
v, Poisson's ratio	0.32
β, Drucker-Prager angle of friction, degrees	55.8
d, Drucker-Prager material cohesion, kPa	10.0
R, cap eccentricity	0.45
$\varepsilon_{vol}^{pl}\Big\|_o$, Initial value of volumetric plastic strain	0.001
K, flow stress ratio	1.0

Hardening law	
Hydrostatic stress, P_b (MPa)	Volumetric Plastic Strain, ε_{vol}^{pl}
0.0082	0
0.0389	0.009
0.0760	0.022
0.1639	0.038
0.3655	0.054
0.7201	0.072

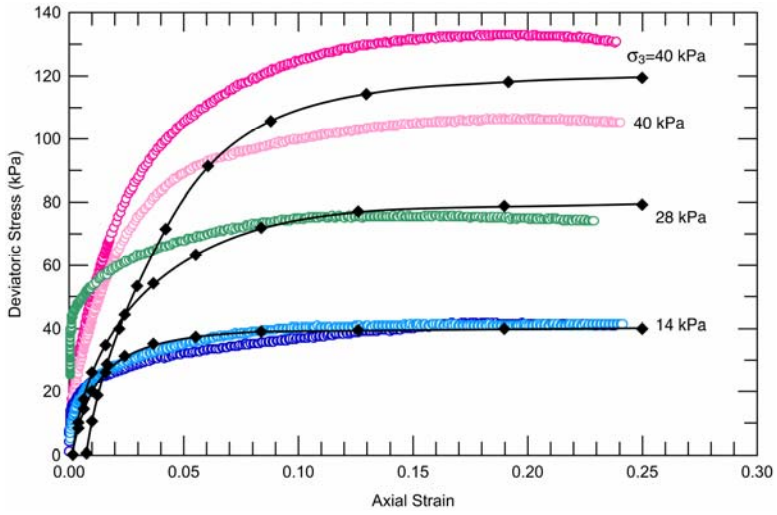

Figure 2: Stress-strain response of Lebanon sand in triaxial loading (○). The confining pressure (σ_3=14, 28, and 40 kPa) is indicted to the right of each curve. The model results are also plotted (–♦–).

4 MODEL VALIDATION

Shoop et al. (2005) validated the CDP model against triaxial test data (Fig. 2). The model matches the stiffness for the lower confining pressure (14 kPa) better than the higher confining pressures (28 and 40 kPa) and does a very good job of predicting the final deviotoric stress values over the entire range of confinining pressures tested. However, this geometry does not probe all aspects of the CDP model. Specifically, the soil in the triaxial test is allowed to expand radially as the sample is loaded axially. This allows the material to fail in shear , but not by compaction. For this reason, we sought to more rigously validate the CDP model using a complex test geometry that induced both compressive and shear failure of the material: the direct shear test (for experimental results see Shoop 1992).

The direct shear test (ASTM D3080-03 Standard Test Method for Direct Shear Test of Soils under Consolidated Drained Conditions) is used to determine the soil cohesion and friction angle used in the Mohr-Coulomb material model. The geometry for this test is shown in Figure 3a. The shear box is split in two halves, the upper half (or top cap) is free to move when a force, *F*, is exerted on it, and the lower half (the bottom cap) is fully constrained. The soil sample is placed in the shear box and a normal load, *N*, is applied to the sample. The ASTM standard allows for rectangular or cylindrical samples; the actual geometry tested in this case is a cylindrical sample taken from a test section in FERF experiments (Shoop 1992). The samples were 6.35 cm in diameter and varied in height (6.35 cm or 7.62 cm). The actual sample height for each test was not consistently reported, regardless, the shear force generally varied over a narrow range, so we choose to model just one sample height: 7.62 cm.

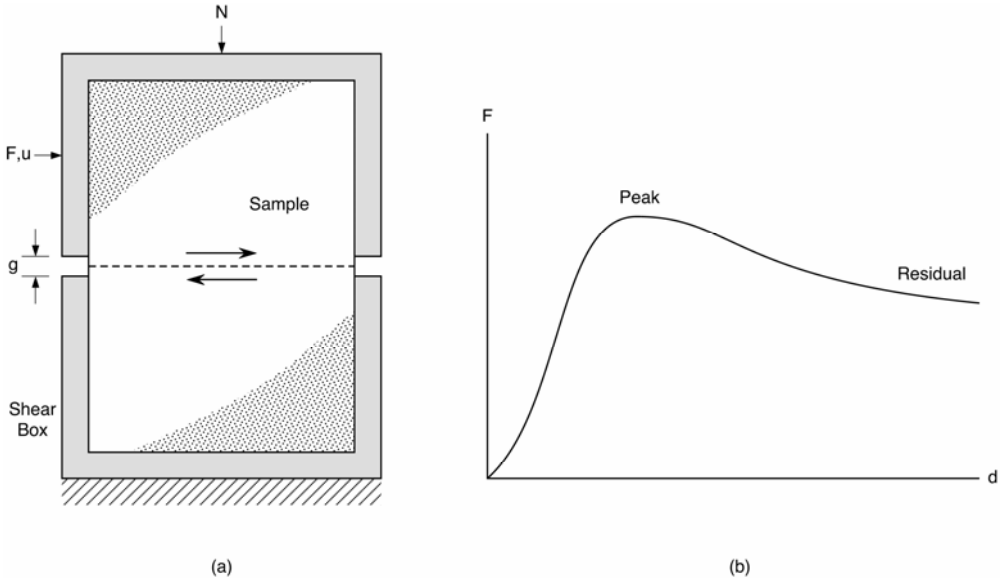

Figure 3: The direct shear test geometry (a) and a typical load trace (b).

Six normal loads were used in the laboratory tests: 21, 112, 243, 360, 556, and 711 N. We replicated each of these load cases in the finite element simulation of this geometry. The normal load was applied as the initial load step and maintained throughout the application of the shear load. After the normal load was applied, the top cap was translated in the horizontal direction at a constant velocity, u=0.08 cm/s—to match the shear velocity in the experiments—while the bottom cap was fully constrained. The height of the top and bottom caps were adjusted for each normal load to maintain a fixed gap (g=1.4 mm) between the caps for all of the simulations. The model mesh was successively refined until the modeled load trace did not vary from one refinement level to the next.

A typical load-displacement curve obtained during the direct shear tests is shown in Figure 3b. In Figure 4 we plot the normalized shear force, $f = F/N$, as a function of top cap displacement. Figures 3b shows that the load rises monotonically, reaches a peak, and subsequently declines and then remains constant at a “residual” value; the finite element simulations consistently reproduced this trend. Also, from Figure 4 we find that, for small normal loads ($N \leq 112$ N), the peak normalized shear force declines as normal load increases. Once the normal load reaches a critical value (112 N < N < 243 N), the peak normalized shear force appears to collapse to a single value ($f_{peak} \sim 0.85$). Finally, the difference between the peak and residual force diminishes with increased normal load.

For comparison, the experimental data (Shoop 1992 and unpublished results from Shoop) are also plotted in Figure 4 and show that the peak loads predicted by the model generally fall within the range of the experimental results and mimick the experimental trends, namely a decline in f_{peak} with increasing normal load until the normal load reaches 243 N, after which f_{peak} remains nearly constant.

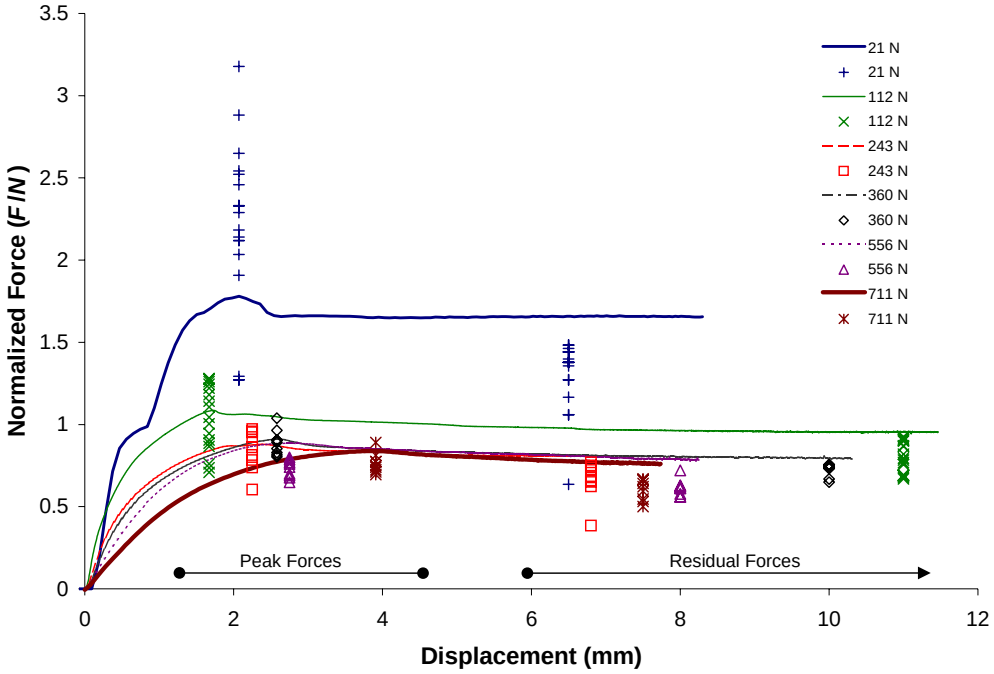

Figure 4: Comparison of finite element simuation of direct shear test with laboratory data.

5 PAVEMENT SIMULATION

We used the CDP thawing soil model to study paved road degradation via thaw. In particular, in this study we looked at the stresses in the pavement and subgrade as the pavement system goes from fully frozen through phases of thawing to fully dry.

In this dynamic simulation the entire depth of the road structure was modeled, the subgrade, base course, and pavement layer, and we simulated passage of the dual tires of a tractor-trailor across the paved surface (Fig. 5). To reduce computational time, the tire was simulated using a rigid analytical surface of 1.06 m diameter and 0.286 m width to represent a Michelin 11 R 22.5 XZY-1 tire. The plane of symmetry is about the center of the dual pair of tires. The vertical load on the wheel is 26.5 kN (for a total axle load of 106 kN). The "soil" was composed of 9 layers, 5 layers of subgrade material, 3 layers of base course, and 1 layer of pavement. The total soil depth modeled is 1.83 m. Details of the layer dimensions are given in Table 2. The material properties of each layer could be changed individually, which allowed for easy modification of the material properties throughout the entire depth of the model to simulate the effects of a receeding frozen layer during the thaw season. The bottom of the model is constrained in the vertical direction. Infinite elements are used on the outer perimeter of the model to reduce model size. The inner "core" of the model uses reduced intergration brick elements.

Twelve individual simulations were conducted for the progression of the thaw layer from the top of the base layer to the bottom of the subgrade (see Table 3).

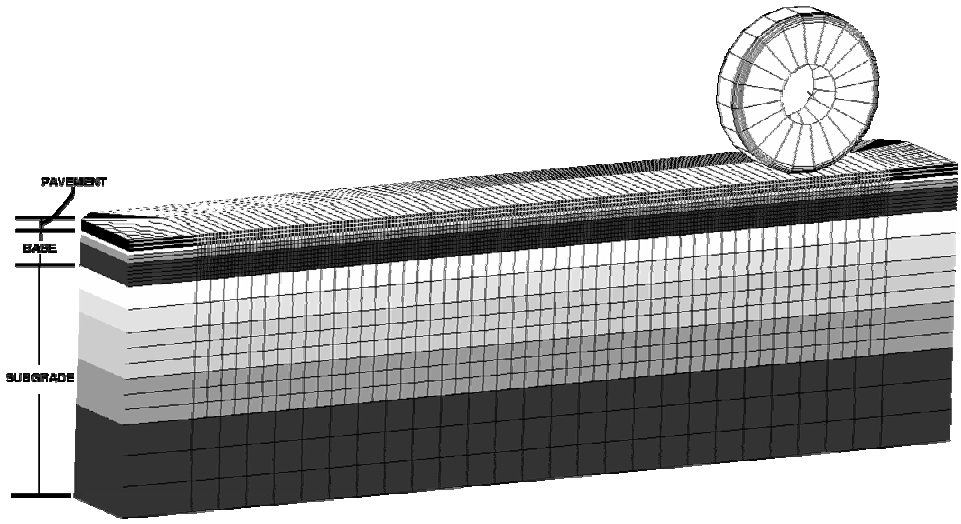

Figure 5: Finite element mesh of pavement rutting model. The shading indicates the location of the sublayers within the subgade, base and pavement layers.

Figure 6 shows the predicted stress at the base of the pavement layer and top of the subgrade as thaw progresses. The left side of the figure shows the winter conditions where the base and subgrade are completely frozen. A thaw layer is introduced in model 2 and progressively migrates deeper though the soil structure until on the right hand side the soil is completely dry (thawed and recovered), representing a summer condition. Owing to bending of the pavement layer under the wheel load, the bottom of the asphalt pavement layer is put into tension. The magnitude of the tensile stress in the horizontal plane is plotted in Figure 6a. This plot shows that the stress level in the pavement layer is not significantly different between winter and summer conditions, yet there is a rapid increase in the stress in the pavement layer as soon as the base course thaws. The stress reaches a maximum when the base course is fully thawed, but not yet started to drain. The tensile stress at the bottom of the pavement begins to reduce as the base layer drains and the thawed layer moves deeper into the soil structure.

Figure 6b shows the vertical stresses at the top of the subgrade as the thaw moves through the soil structure. Clearly, the tensile stresses seem unaffected by the thaw progression. The compressive stresses at the top of the subgrade layer peak as soon as thaw begins, and decline continuously as the thaw moves down through the structure. In fact, it appears that the peak compaction stresses occur while the subgrade is at its strongest, i.e., frozen. Once the thaw depth reaches the subgrade layer, the compression stresses decline significantly and continue to subside until the structure has completely thawed and dried.

This simulation shows that the pavement is placed under the greatest stress when the base course is the weakest from being fully thawed and not yet drained (recovered). Furthermore the level of tensile stress at the base of the asphalt layer during thaw is over four times that experianced during the summer season. Also, the lateral stresses (transverse to the roadway) are typically 30% higher than the longitudinal stresses. This is consitant with the cracking pattern in the pavement being normal to the direction of maximum stress (i.e., normal to the lateral direction) as shown by the longitudinal cracking in Figure 1.

Table 2: Dimensions of layers and elastic properties of the materials used in the pavement model. The plastic properties for the thawed layer (T) are given inTable 1.

Layer	Sublayer	Layer Thickness (cm)	Depth of top of layer (cm)
Pavement		7.62	0
Base	3	2.54	7.62
	2	5.08	10.16
	1	15.24	15.24
Subgrade	5	15.24	30.48
	4	15.24	45.72
	3	30.48	60.96
	2	30.48	91.44
	1	60.96	121.92

Material	Elastic Modulus (MPa)	Poissons Ratio	Density (kg/m3)	Abbreviation
Pavement	2758	0.3	3000	P
Base-dry	275.8	0.4	2000	B
Base-frozen	413.7	0.25	1600	F
Subgrade-dry	1.207	0.4	1762	S
Subgrade-frozen	413.7	0.25	1600	F
Thawed layer	0.0085	0.32	1890	T

Table 3: Description of the models run to study pavement and subgrade stress due to thawing. Abreviations for layering given in Table 2.

Model #	Layering	Description
1	PFFFFFFFF	Entire structure frozen (winter condition)
2	PTFFFFFFF	Top 2.54 cm of base layer thawed
3	PTTFFFFFF	Top 7.62 cm of base layer thawed
4	PTTTFFFFF	Entire base layer thawed
5	PBTTFFFFF	Top 2.54 cm of base layer dry, remainder thawed
6	PBBTFFFFF	Top 7.62 cm of base layer dry, remainder thawed
7	PBBBTFFFF	Entire based layer dry, top 15.24 cm of subgrade thawed
8	PBBBSTFFF	Thawed layer is at 122-173 cm within subgrade
9	PBBBSSTFF	Thawed layer is at 91-122 cm within subgrade
10	PBBBSSSTF	Thawed layer is at 61-91 cm within subgrade
11	PBBBSSSST	Thawed layer is at bottom of subgrade
12	PBBBSSSSS	Entire structure thawed and dry (summer condition)

6 CONCLUSIONS

The modified Capped Drucker-Prager constituative law was used for modeling the material behavior of a thawing soil using the finite element method. Available triaxial laboratory data were used to obtain suitable material parameters and to calibrate the model.

The thawing soil model was validated by simulating the direct shear tests. This simulation faithfully reproduced the response of the soil under this complicated load case. In particular it predicted the decline in peak normalized shear force with increasing normal load as well as the overall shape of the force displacement curve.

This model was used to simulate a pavement system subjected to a thaw cycle. This simulation modeled the progression of thaw from frozen winter conditions through initial thawing of the top of the base layer followed by migration of the thaw layer deeper into the soil until the entire depth of the structure was completely thawed and dry (summer conditions). This simulation showed that the pavement is most severly distressed when the base course is completely thawed. Once the base course is dry and the thawing layer has migrated into the subgrade material, the stress in the pavement declines significantly. This

model will be used to understand the effects of thaw on the pavement systems, with the goal of optimizing the soil structure to minimize the affects of thaw on pavement failure.

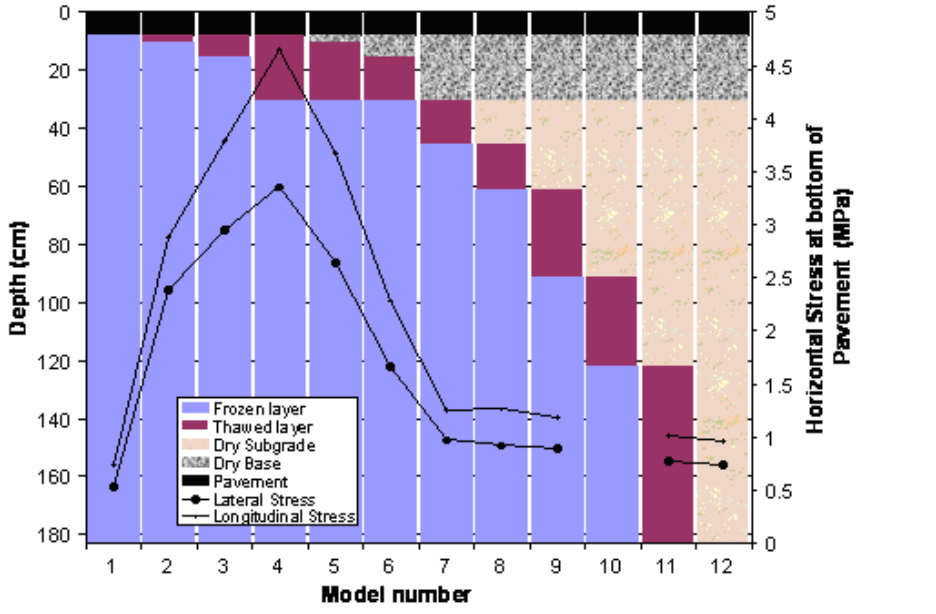

(a)

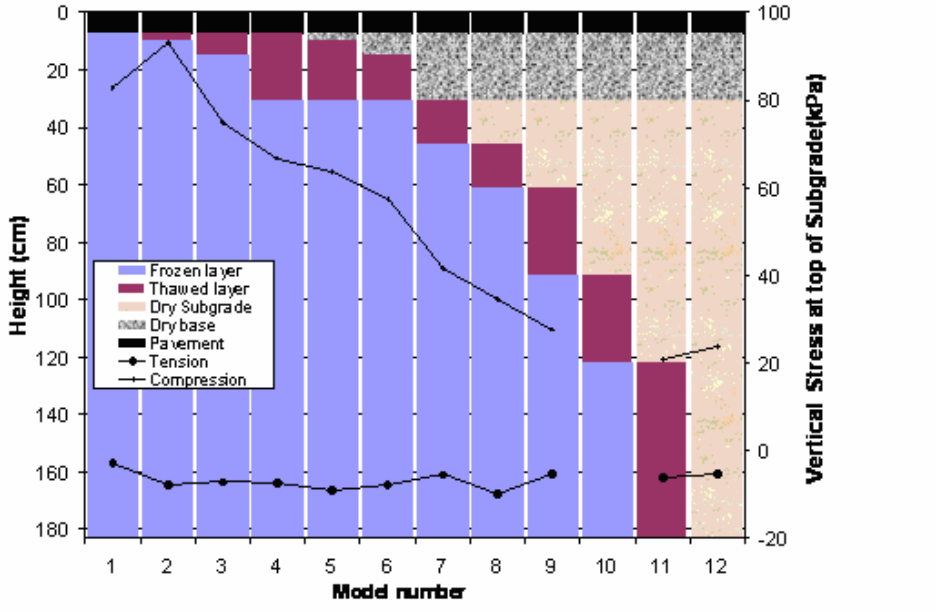

(b)

Figure 6: Predicted (a) maximum horizontal stress at base of pavement layer and (b) maximum vertical stress at top of subgrade, under the wheel centerline. Bars show layering of pavement structure.

7 ACKNOWLEDGEMENTS

This work was funded by the U.S. Army under the Airfields and Pavements Program and the Joint Rapid Airfield Construction Program. The authors would like to thank James Tantillo for his help preparing the direct shear finite element models.

REFERENCES

HKS (Hibbitt, Karlsson & Sorensen, Inc.), 1998. *ABAQUS Theory and User's Manuals*. Pawtucket, Rhode Island.

Janoo, V.C, and Berg, R.L., 1990a. *Predicting the behavior of asphalt concrete pavements in seasonal frost areas using nondestructive techniques*. CRREL Report 90-10, U.S. Army Cold Regions Research and Engineering Laboratory.

Janoo, V, and Berg, R., 1990b. *Thaw weakening of pavement structures in seasonal frost areas*. Transportation Research Record No. 1286, Transportation Research Board, p 217–233.

Janoo, V. and Shoop, S., 2004. *Influence of Spring Thaw on Pavement Rutting*, submitted to UNBAR6 -Pavements Unbound, Nottingham, UK, July 2004, p. 115-124.

Saarelainen, S., Onninen, H., Kangas, H., & Pihlajamaki, J., 1999. *Full-scale accelerated testing of a pavement on thawing, frost-susceptible subgrade (CS8-3)*. International Conference on the Accelerated Pavement Testing, Oct. 18–20, 1999, Reno, Nevada www.tieh.fi/tppt/hvsr

Shoop, S.A., 1988. *Research Plan and Experimental Design for the Study of Vehicle Mobility in Thawing Soils*. Internal Report 1001, CRREL, Hanover, NH.

Shoop, S.A., 1990. *Mechanisms controlling vehicle mobility on a thawing soil*. Proceedings 10th International Conference of the ISTVS, Kobe, Japan, August 20-24.

Shoop, S.A., 1992. *Comparison of thawing soil strength measurements for predicting vehicle performance*. CRREL Report 92-17, Cold Regions Research and Engineering Laboratory, Hanover, NH.

Shoop, S.A., 1993. *Thawing Soil Strength Measurements for Predicting Vehicle Performance*. J. Terramechanics, Vol. 30, No. 6, PP. 405-418.

Shoop, S.A., Affleck, R., Janoo, V., Haehnel, R., Bartlett., B., 2005. *Constitutive model for thawing, frost susceptible sand*. ERDC/CRREL Report TR-05-3.

Shoop, S.A., and Bigl S.R., 1997 *Moisture Migration During Freeze and Thaw of Unsaturated Soils: Modeling and Large Scale Experiments*. Cold Regions Science and Technology, Vol. 25, pg. 33-45.

Shoop, S.A. and Henry, K.S., 1991. *The Effect of a Geotextile on Water Migration and Frost Heave in a Large Scale Test Basin*. Transportation Research Record 1307, p. 309-318.

Zhang, W., & Macdonald, R.A., 2002. *The effects of freeze-thaw periods on a test pavement in the Danish road testing machine*. 9th International Conference on Asphalt Pavements, Aug. 17–22, 2002, Copenhagen, Denmark. Published by the International Society for Asphalt Pavements, 2002, CD-ROM, 20 http://www.ctt.dtu.dk/group/rtm/ISAP_Paper338_Zhang.pdf